

# PACMANN: Point Adaptive Collocation Method for Artificial Neural Networks

Coen Visser<sup>a</sup>, Alexander Heinlein<sup>b,\*</sup>, Bianca Giovanardi<sup>a,c</sup>

<sup>a</sup>Faculty of Aerospace Engineering, Delft University of Technology, 2629 HS Delft, The Netherlands

<sup>b</sup>Delft Institute of Applied Mathematics, Faculty of Electrical Engineering, Mathematics and Computer Science, Delft University of Technology, 2628 CD Delft, The Netherlands

<sup>c</sup>Delft Institute for Computational Science and Engineering, Delft University of Technology, 2628 CD, The Netherlands

---

## Abstract

Physics-Informed Neural Networks (PINNs) are an emerging tool for approximating the solution of Partial Differential Equations (PDEs) in both forward and inverse problems. PINNs minimize a loss function which includes the PDE residual determined for a set of collocation points. Previous work has shown that the number and distribution of these collocation points have a significant influence on the accuracy of the PINN solution. Therefore, the effective placement of these collocation points is an active area of research. Specifically, adaptive collocation point sampling methods have been proposed, which have been reported to scale poorly to higher dimensions. In this work, we address this issue and present the Point Adaptive Collocation Method for Artificial Neural Networks (PACMANN). Inspired by classic optimization problems, this approach incrementally moves collocation points toward regions of higher residuals using gradient-based optimization algorithms guided by the gradient of the squared residual. We apply PACMANN for forward and inverse problems, and demonstrate that this method matches the performance of state-of-the-art methods in terms of the accuracy/efficiency tradeoff for the low-dimensional problems, while outperforming available approaches for high-dimensional problems; the best performance is observed for the Adam optimizer. Key features of the method include its low computational cost and simplicity of integration in existing physics-informed neural network pipelines.

*Keywords:* Differential equations, Physics-informed neural networks (PINNs), Adaptive sampling, Residual gradient

---

## 1. Introduction

Physics-Informed Neural Networks (PINNs) build upon the ability of deep neural networks to serve as universal function approximators, as established by Hornik et al. [1] in 1989. Based on this finding, several methods were developed to solve Ordinary Differential Equations (ODEs)

---

\*Corresponding author

Email address: A.Heinlein@tudelft.nl (Alexander Heinlein)

and Partial Differential Equations (PDEs) using neural networks, originally proposed by [2, 3]. Supported by these developments and recent advances in computational tools, notably automatic differentiation in 2015 [4], Raissi et al. [5] proposed the name and framework of physics-informed neural networks in 2019 and their use to approximate the solution of PDEs in both forward and inverse problems. In their classic form, PINNs approximate the solution by minimizing a loss function based on boundary conditions, initial conditions, and the PDE residual sampled over a set of collocation points. In the following years, PINNs have been applied in a variety of fields [6, 7], such as fluid dynamics [8, 9, 10], heat transfer [11, 12], material sciences [13, 14] and electromagnetism [15, 16].

In 2020, Mao et al. [8] explored the impact of collocation point placement on prediction accuracy for solutions with discontinuities. They demonstrated that, when discontinuities are known a priori, manually increasing the density of points near these regions improves prediction accuracy. To address scenarios where solution features are unknown before training, adaptive algorithms for collocation point selection were developed. For instance, Lu et al. [17] introduced Residual-based Adaptive Refinement (RAR) in 2021, the first adaptive sampling algorithm, which places additional points in regions with the largest PDE residuals. RAR improves prediction accuracy, capturing features such as a discontinuity in a Burgers' equation problem better than a static grid. Instead of sampling points only where the residual is the largest, Nabian et al. [18] proposed to randomly resample all points in the domain based on a Probability Density Function (PDF) proportional to the residual. This approach samples a higher density of points in high residual areas, resulting in accelerated convergence of the PINN. Based upon these studies, Wu et al. [19] presented two additional sampling algorithms, Residual-based Adaptive Distribution (RAD) and Residual-based Adaptive Refinement with Distribution (RAR-D). In RAD, all collocation points are resampled using a PDF based on the residual. RAR-D is a combination of RAR and RAD, where collocation points are sampled in addition to the existing collocation points according to the same probability density function used by RAD. Both approaches lead to a higher prediction accuracy, specifically for PDEs with complex solutions due to, for example, steep gradients. Moreover, RAD was found to outperform the method proposed by Nabian et al. [18].

Several adaptations to the aforementioned PDF-based sampling algorithms have been proposed. Guo et al. [20], for example, state that adaptive sampling methods should obey temporal causality. They propose the adaptive causal sampling method, which decomposes the domain into subdomains where the ratio of points sampled in each subdomain is based on the PDE residual and a temporal weight, ensuring temporal causality. This approach was found to enhance the prediction accuracy and computational efficiency of PINNs in problems with nonlinear PDEs containing higher-order derivatives. Furthermore, Mao et al. [21] consider the gradient of the solution by sampling additional points in subdomains with large residuals and large solution gradients. Liu et al. [22] propose to add points with large residual gradients to the set of collocation points used for training. Both Mao et al. and Liu et al. report an improvement in accuracy for problems with solutions exhibiting steep gradients.

While the aforementioned collocation point sampling methods have proven effective in low-dimensional problems, these approaches to resampling are computationally expensive for high-dimensional problems as reported by Wu et al. [19]. Methods such as RAD or RAR are computationally expensive for these problems due to the cost of evaluating the residual in a sufficiently

large number of points, either to construct the probability density function or to identify additional points for inclusion in the training process.

Other approaches have been proposed to sample collocation points in high-dimensional problems. For instance, Tang et al. [23] propose the DAS-PINNs approach, which samples according to a Deep Adaptive Sampling (DAS) method and uses KRnet [24], a deep generative model, to approximate the PDF proportional to the residual. However, this approach is complex to implement in existing PINNs pipelines due to its dual-network framework.

The present work aims to develop a collocation point resampling method that efficiently scales to higher dimensions without introducing significant computational overhead while maintaining the advantages of previous approaches. We propose the Point Adaptive Collocation Method for Artificial Neural Networks (PACMANN), which uses the gradient of the squared residual to move collocation points toward areas with a large residual. In this approach, collocation point resampling is formulated as a maximization problem of the squared residual, where established optimization methods may be employed to move points. PACMANN includes two main hyperparameters, the stepsize and the number of steps taken by the optimization algorithm.

First, we investigate the performance of PACMANN in combination with a variety of optimization algorithms for two low-dimensional problems: a 1D Burgers' equation and a 1D Allen-Cahn equation. We then perform sensitivity studies for the number of collocation points, the number of iterations between resampling, and the two aforementioned hyperparameters of our proposed method. In addition, we demonstrate the suitability of PACMANN to high-dimensional and inverse problems: a 5D Poisson's equation and a 2D inverse Navier-Stokes equation. For all problems under consideration, we compare the performance of our method in terms of prediction accuracy and computational cost to state-of-the-art adaptive and non-adaptive sampling methods. Notably, our results show that our method matches the performance of state-of-the-art methods in terms of the accuracy/efficiency tradeoff for low-dimensional problems and efficiently scales to high-dimensional problems, where it outperforms state-of-the-art methods.

This paper is organized as follows. In Section 2, a review of the PINNs framework is given, followed by a description of PACMANN and the optimization algorithms considered in this study. Next, in experimental studies in Section 3, we compare the accuracy and computational cost of PACMANN to other sampling methods for three forward problems and an inverse problem under varying hyperparameters. Finally, in Section 4, we summarize our findings.

## 2. Methodology

This section begins with a brief review of PINNs based on the framework presented by Raissi et al. [5] in 2019. Next, we propose the novel PACMANN, followed by a summary of the optimization algorithms considered in this work.

### 2.1. Physics-Informed Neural Networks

PINNs approximate the solution of PDEs using neural networks. Generally, we consider PDEs of the form

$$\mathbf{u}_t + \mathcal{N}[\mathbf{u}] = 0, \quad \mathbf{x} \in \Omega, \quad t \in [0, T],$$

with the initial and boundary conditions

$$\begin{aligned} \mathbf{u}(\mathbf{x}, 0) &= h(\mathbf{x}), \quad \mathbf{x} \in \Omega, \\ \mathcal{B}[\mathbf{u}](\mathbf{x}, t) &= 0, \quad \mathbf{x} \in \partial\Omega, \quad t \in [0, T], \end{aligned}$$

where  $\mathcal{N}[\cdot]$  is a linear or nonlinear differential operator, and  $\mathcal{B}[\cdot]$  is a boundary operator corresponding to a set of boundary conditions. In addition,  $\mathbf{x} \in \mathbb{R}^d$  and  $t \in [0, T]$  denote the spatial and temporal coordinates,  $\Omega \subset \mathbb{R}^d$ ,  $\partial\Omega$  forms the boundary. The set of collocation points  $\{\mathbf{x}_r^i, t_r^i\}_{i=1}^{N_r}$  in the domain  $\mathcal{D}$  are represented by  $\mathbf{X}$ . Furthermore,  $\mathbf{u}$  denotes the exact solution.

The PINN consists of a (deep) neural network with the coordinates  $(\mathbf{x}, t)$  as inputs and  $\hat{\mathbf{u}}(\mathbf{x}, t, \boldsymbol{\theta})$  as output. The trainable parameters  $\boldsymbol{\theta}$  of this neural network are trained by minimizing the loss function  $\mathcal{L}(\boldsymbol{\theta})$

$$\boldsymbol{\theta}^* = \arg \min_{\boldsymbol{\theta}} \mathcal{L}(\boldsymbol{\theta}).$$

The loss function is defined as

$$\mathcal{L}(\boldsymbol{\theta}) = \lambda_r \mathcal{L}_r(\boldsymbol{\theta}) + \lambda_{ic} \mathcal{L}_{ic}(\boldsymbol{\theta}) + \lambda_{bc} \mathcal{L}_{bc}(\boldsymbol{\theta}), \quad (1)$$

where

$$\begin{aligned} \mathcal{L}_r(\boldsymbol{\theta}) &= \frac{1}{N_r} \sum_{i=1}^{N_r} \left( \hat{\mathbf{u}}_t(\mathbf{x}_r^i, t_r^i, \boldsymbol{\theta}) + \mathcal{N}[\hat{\mathbf{u}}](\mathbf{x}_r^i, t_r^i, \boldsymbol{\theta}) \right)^2, \\ \mathcal{L}_{ic}(\boldsymbol{\theta}) &= \frac{1}{N_{ic}} \sum_{i=1}^{N_{ic}} \left( \hat{\mathbf{u}}(\mathbf{x}_{ic}^i, 0, \boldsymbol{\theta}) - h(\mathbf{x}_{ic}^i) \right)^2, \\ \mathcal{L}_{bc}(\boldsymbol{\theta}) &= \frac{1}{N_{bc}} \sum_{i=1}^{N_{bc}} \left( \mathcal{B}[\hat{\mathbf{u}}](\mathbf{x}_{bc}^i, t_{bc}^i, \boldsymbol{\theta}) \right)^2. \end{aligned}$$

Here,  $\mathcal{L}_r$ ,  $\mathcal{L}_{ic}$ , and  $\mathcal{L}_{bc}$  represent the loss terms for the PDE residual, initial conditions, and the boundary conditions, respectively. Furthermore,  $N_r$ ,  $N_{ic}$ , and  $N_{bc}$  denote the number of collocation points of the aforementioned terms. The hyperparameters  $\lambda_r$ ,  $\lambda_{ic}$ , and  $\lambda_{bc}$  are scalar weights used to balance the loss function. Each loss term is evaluated over a set of data points, where  $\{\mathbf{x}_r^i, t_r^i\}_{i=1}^{N_r}$  is a set of collocation points located in the interior of the domain,  $\{\mathbf{x}_{ic}^i\}_{i=1}^{N_{ic}}$  is a set of points sampled at the initial time, and  $\{\mathbf{x}_{bc}^i, t_{bc}^i\}_{i=1}^{N_{bc}}$  is a set sampled along the boundary. These points may be fixed during training, resampled through periodic random resampling, or resampled using adaptive sampling methods based on guiding information, such as the PDE residual.

To train the model parameters  $\boldsymbol{\theta}$ , the gradient of the loss function with respect to the parameters is determined using back-propagation [25]. Next, the model parameters are updated with an optimization algorithm, often based on the gradient descent method, such as the Adam optimizer [26]. Similarly, the gradients of  $\mathbf{u}(\mathbf{x}, t, \boldsymbol{\theta})$  with respect to the input coordinates  $(\mathbf{x}, t)$  as required by  $\mathcal{N}[\cdot]$  and potentially  $\mathcal{B}[\cdot]$  in equation (1) are computed using automatic differentiation.

For problems that incorporate reference data during training, such as inverse problems, an additional loss term  $\mathcal{L}_{ref}$  is added to the loss function described by equation (1), where

$$\mathcal{L}_{ref}(\boldsymbol{\theta}) = \frac{1}{N_{ref}} \sum_{i=1}^{N_{ref}} \left( \hat{\mathbf{u}}(\mathbf{x}^i, t^i, \boldsymbol{\theta}) - \mathbf{u}_{ref}(\mathbf{x}^i, t^i) \right)^2.$$

This term corresponds to the mean squared error between the (noisy) observed data  $\mathbf{u}_{ref}$  at the set of data points  $\{\mathbf{x}^i, t^i\}_{i=1}^{N_{ref}}$  and the approximation  $\hat{\mathbf{u}}(\mathbf{x}^i, t^i, \boldsymbol{\theta})$  given by the neural network. The addition of this term leads to the following loss function

$$\mathcal{L}(\boldsymbol{\theta}) = \lambda_r \mathcal{L}_r(\boldsymbol{\theta}) + \lambda_{ic} \mathcal{L}_{ic}(\boldsymbol{\theta}) + \lambda_{bc} \mathcal{L}_{bc}(\boldsymbol{\theta}) + \lambda_{ref} \mathcal{L}_{ref}(\boldsymbol{\theta}),$$

where  $\lambda_{ref}$  is the scalar weight assigned to the reference data loss term.

## 2.2. Point Adaptive Collocation Method for Artificial Neural Networks

In this work, we propose PACMANN which uses the gradient of the squared residual as guiding information in combination with established optimization algorithms to gradually move collocation points toward areas of high residuals; see Algorithm 1 and Figure 1. This method turns collocation point resampling into a maximization problem. Training the model parameters  $\boldsymbol{\theta}$  can thus be formulated as the following min-max problem

$$\boldsymbol{\theta}^* = \arg \min_{\boldsymbol{\theta}} \left[ \lambda_{ic} \mathcal{L}_{ic}(\boldsymbol{\theta}) + \lambda_{bc} \mathcal{L}_{bc}(\boldsymbol{\theta}) + \lambda_{ref} \mathcal{L}_{ref}(\boldsymbol{\theta}) + \max_{\mathbf{X} \subset \mathcal{D}} \lambda_r \mathcal{L}_r(\mathbf{X}, \boldsymbol{\theta}) \right].$$

Where only the collocation points are moved, while points such as those sampled along the boundary are fixed in place throughout training. This approach ensures that a sufficient number of points are placed along the initial and boundary conditions to accurately compute the respective loss terms.

First,  $N_r$  collocation points are sampled using a uniform sampling method, such as an equi-spaced uniform grid or the Hammersley sequence [27]. The PINN is then trained on this set of collocation points for a number of iterations determined by the resampling period  $P$ . Next, training is stopped and the gradients of the squared residual  $r^2(\mathbf{x}, t)$  with respect to the input coordinates, given by  $\nabla_{\mathbf{x}} r^2(\mathbf{x}, t)$  and  $\frac{\partial}{\partial t} r^2(\mathbf{x}, t)$ , are determined for each collocation point  $(\mathbf{x}, t)$ . The collocation points are subsequently moved in the direction of increasing residual based on the direction and magnitude of the residual gradient, as described by

$$\begin{cases} \mathbf{x}_r^{i+1} = \mathbf{x}_r^i + s \cdot \nabla_{\mathbf{x}} r^2(\mathbf{x}_r^i, t_r^i) \\ t_r^{i+1} = t_r^i + s \cdot \frac{\partial}{\partial t} r^2(\mathbf{x}_r^i, t_r^i). \end{cases} \quad (2)$$

Here,  $s$  determines the stepsize of each move. Since training is stopped, the residual landscape is static and the residual gradient can be determined again for the new location of the collocation point, allowing the process to be repeated. Therefore, collocation points can be moved several times, given by the number of steps  $T$ . If a point moves outside the domain, it is removed and a replacement point is sampled in the domain based on a uniform probability distribution. Next, the neural network is trained for another  $P$  iterations, after which the process of moving collocation points is repeated.

In equation (2), points are moved directly based on the gradient vector. This approach is essentially equal to applying gradient ascent. However, other gradient-based optimization algorithms can be applied. The optimization algorithms considered for PACMANN in Section 3 are listed as follows, with examples for an arbitrary variable  $x$  and a function  $f(x)$  to be maximized.

---

**Algorithm 1: PACMANN with  $P$ ,  $s$  and  $T$** 

---

- 1 Sample a set  $X$  of  $N_r$  collocation points  $\{\mathbf{x}_r^i, t_r^i\}_{i=1}^{N_r}$  using a uniform sampling method;
  - 2 **repeat**
  - 3     Train the PINN for  $P$  iterations;
  - 4     Determine  $r^2(\mathbf{x}, t) = \left( \mathbf{u}_t(\mathbf{x}_r^i, t_r^i, \boldsymbol{\theta}) + \mathcal{N}[\mathbf{u}](\mathbf{x}_r^i, t_r^i, \boldsymbol{\theta}) \right)^2$ , the squared PDE residual over  $X$ ;
  - 5     Find  $\nabla_{\mathbf{x}} r^2(\mathbf{x}, t)$  and  $\frac{\partial}{\partial t} r^2(\mathbf{x}, t)$ , the gradients of the squared PDE residual with respect to the input coordinates of the points in  $X$ ;
  - 6     Iteratively move the points in  $X$  according to the chosen optimization algorithm with stepsize  $s$  and number of steps  $T$ ;
  - 7     Replace points in  $X$  outside the domain with points sampled according to a uniform probability distribution;
  - 8 **until** the total number of iterations reaches the limit;
- 

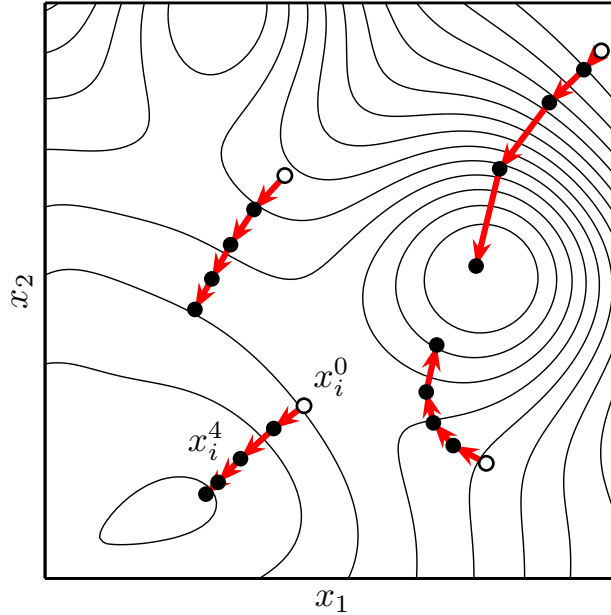


Figure 1: A schematic of PACMANN with five steps of gradient ascent on a contour plot of the squared residual.

1. **Gradient ascent:** The collocation points are directly moved in the direction of steepest ascent. This algorithm updates variables using the principle:

$$x_{i+1} = x_i + s \cdot \frac{d}{dx}f(x_i).$$

2. **Nonlinear gradient ascent:** In this algorithm, we apply a nonlinear function to the gradient ascent algorithm to scale down large gradients, preventing points from taking large steps directly out of the domain. We refer to the algorithm as nonlinear gradient ascent. In this work, we use the hyperbolic tangent function, as shown in the example:

$$x_{i+1} = x_i + s \cdot \tanh\left(\frac{d}{dx}f(x_i)\right).$$

3. **RMSprop [28]:** RMSprop adapts the stepsize by dividing the gradient by a weighted average of previous gradients; this serves to stabilize convergence. The algorithm consists of two steps. First, a parameter  $S$  is updated. This parameter consists of a weighted average of previous gradients:

$$S_{i+1} = \beta \cdot S_i + (1 - \beta) \cdot \left(\frac{d}{dx}f(x_i)\right)^2.$$

Here,  $\beta$  influences the weight of the current gradient, set to 0.999. Furthermore,  $S_0$  is set to 0. Next, the variable  $x_i$  is updated using:

$$x_{i+1} = x_i + s \cdot \frac{\frac{d}{dx}f(x_i)}{\sqrt{S_{i+1} + \epsilon}}.$$

To prevent large steps due to small values of  $S$ , a small value ( $10^{-8}$ ) is added, represented by  $\epsilon$ .

4. **Momentum [29]:** The momentum optimizer considers a weighted average of previous gradients at each iteration to prevent converging to local minima. First, the weighted average is computed, represented by  $V$ :

$$V_{i+1} = \beta \cdot V_i + (1 - \beta) \cdot \left(\frac{d}{dx}f(x_i)\right).$$

Here,  $V_0$  is set to 0 and  $\beta$  to 0.9. After updating  $V$ , the variable  $x$  is updated:

$$x_{i+1} = x_i + s \cdot V_{i+1}.$$

5. **Adam [26]:** The Adam optimizer combines the concepts behind momentum and RMSprop. First, the value of  $V$  is updated:

$$V_{i+1} = \beta_1 \cdot V_i + (1 - \beta_1) \cdot \frac{d}{dx}f(x_i).$$

Here,  $\beta_1$  is set to 0.9 and  $V_0$  to 0. Next, the parameter  $S$  is updated:

$$S_{i+1} = \beta_2 \cdot S_i + (1 - \beta_2) \cdot \left( \frac{d}{dx} f(x_i) \right)^2.$$

Here,  $\beta_2$  is set to 0.999. Afterwards, an initialization bias correction is applied to  $V_{i+1}$  and  $S_{i+1}$ :

$$\hat{V}_{i+1} = \frac{V_{i+1}}{1 - \beta_1^{i+1}}, \quad \hat{S}_{i+1} = \frac{S_{i+1}}{1 - \beta_2^{i+1}}.$$

Finally, the variable  $x$  is updated as follows:

$$x_{i+1} = x_i + s \cdot \frac{\hat{V}_{i+1}}{\sqrt{\hat{S}_{i+1} + \epsilon}}$$

Here,  $\epsilon$  is set to  $10^{-8}$ , preventing large steps when  $\hat{S}_{i+1}$  is small.

6. **Golden section search [30]:** Golden section search is a line search method that narrows down the search interval each iteration. By searching along the direction of steepest ascent, the multidimensional optimization problem is reduced to a one-dimensional problem. In this direction, the algorithm searches in an interval  $[a_i, b_i]$ . In the initial interval,  $a_0$  is equal to the value  $x_0$ , for example, the x-coordinate of a collocation point. We determine  $b_0$  using the stepsize and the gradient:

$$b_0 = a_0 + s \cdot \frac{d}{dx} f(x_0).$$

Next,  $f(x)$  is evaluated at two points,  $x_{l,i}$  and  $x_{r,i}$ , determined using:

$$x_{l,i} = a_i + \alpha \cdot (b_i - a_i), \quad x_{r,i} = a_i + \beta \cdot (b_i - a_i).$$

The name "golden section search" refers to the golden ratio, defined as  $\phi = \frac{1+\sqrt{5}}{2}$ , which is incorporated in the values of  $\alpha$  and  $\beta$ :

$$\alpha = 1 - \phi^{-1}, \quad \beta = \phi^{-1}$$

If  $f(x_{l,i}) > f(x_{r,i})$ , then the interval is shortened and shifted to the left:

$$a_{i+1} = a_i, \quad b_{i+1} = x_{r,i}, \quad x_{r,i+1} = x_{l,i}.$$

Else, if  $f(x_{l,i}) < f(x_{r,i})$ , then the interval is shortened and shifted to the right:

$$a_{i+1} = x_{l,i}, \quad b_{i+1} = b_i, \quad x_{l,i+1} = x_{r,i}.$$

After updating the interval to  $[a_{i+1}, b_{i+1}]$ , the algorithm is repeated again. After the final iteration, the value of the variable  $x$  is found by taking the middle point of the interval  $[a_N, b_N]$ :

$$x_N = \frac{a_N + b_N}{2}.$$

The golden ratio ensures that either  $x_{l,i+1}$  ends up on  $x_{r,i}$  or  $x_{r,i+1}$  on  $x_{l,i}$ , depending on the direction of the interval shift. Since  $f(x)$  has already been determined for  $x_{l,i}$  and  $x_{r,i}$  in the previous iteration,  $f(x)$  does not have to be evaluated again for these variable values. As a result, for each iteration, the value of  $f(x)$  only has to be evaluated once, lowering the computational cost.



### 3. Results

In this section, PACMANN is compared to collocation point sampling methods proposed in related work [17, 19]. In the following tables and figures, PACMANN is denoted by an asterisk (\*) followed by the optimization method used, for example, “\*Adam”. In addition, the hyperparameters of PACMANN are varied to showcase its behavior. To gather data on the prediction accuracy and computational cost, each method and set of hyperparameters is run ten times. The prediction accuracy is compared based on the mean and standard deviation of the test error, measured using the  $L_2$  relative error. The  $L_2$  relative error is determined as follows:

$$L_2 = \frac{\|\mathbf{u}_{true} - \mathbf{u}_{pred}\|_2}{\|\mathbf{u}_{true}\|_2}, \quad (3)$$

where  $\mathbf{u}_{true}$  is the true solution and  $\mathbf{u}_{pred}$  is the predicted solution. In the following numerical experiments,  $\mathbf{u}_{true}$  and  $\mathbf{u}_{pred}$  are compared over an equispaced uniform grid of 10,000 collocation points. The mean runtime of training over the ten runs serves as an indication of the computational cost of a particular sampling method. All numerical experiments were carried out with the PINNs library DeepXDE [17] using PyTorch [31] version 1.12.1 as the backend. The PINNs were trained using NVIDIA Tesla V100S GPUs on TU Delft’s high-performance computer DelftBlue [32].

For all experiments, the neural network is trained in five identical blocks of 10,000 iterations, consisting of 7000 iterations of Adam with a learning rate of  $10^{-3}$  followed by 3000 iterations of L-BFGS, totaling 50,000 iterations. Throughout training, a resampling period  $P$  of 50 iterations is maintained. Furthermore, resampling only occurs when Adam is set as the optimizer of the neural network. Resampling while L-BFGS is optimizer would disrupt the convergence of the algorithm due to the change in loss landscape by evaluating the PDE loss term at different collocation points. In this work, the hyperbolic tangent is used as activation function.

In the numerical experiments, PACMANN with Adam consistently achieves the lowest error compared to the other optimization algorithms considered. Therefore, to preserve clarity, figures and tables which compare the various sampling methods only contain the results for Adam with our method. The figures comparing the accuracy behavior of the other optimization algorithms discussed in Section 2 for varying numbers of collocation points and resampling periods are provided in Appendix A.

Infrequently, the random neural network weight initialization prevents the PINN from learning the solution, which results in a test error several orders of magnitude larger than the test error obtained with other weight initializations. This has been observed for all sampling methods considered in this study and is characterized by volatile loss behavior or large static loss terms. When this occurs, the results are not considered and the PINN is trained for ten different network initializations to gather new results.

#### 3.1. 1D Burgers’ equation

We first consider the 1D Burgers’ equation:

$$\begin{cases} \frac{\partial u}{\partial t} + u \frac{\partial u}{\partial x} = \nu \frac{\partial^2 u}{\partial x^2}, & x \in [-1, 1], \quad t \in [0, 1] \\ u(x, 0) = -\sin(\pi x) \\ u(-1, t) = u(1, t) = 0. \end{cases} \quad (4)$$

Here,  $\nu$  is the diffusion coefficient or kinematic viscosity, set at  $\nu = 0.01/\pi$ . For this problem, the number of collocation points is set to 2500, the number of points on the boundary to 80, and the number of points on the initial condition to 160. The neural network architecture used for this example consists of four hidden layers of 64 neurons.

Sampling method	$L_2$ relative error		Mean runtime [s]
	Mean	1 SD	
Uniform grid	25.9%	14.2%	425
Hammersley grid	0.61%	0.53%	443
Random resampling	0.40%	0.35%	<b>423</b>
RAR	0.11%	<b>0.05%</b>	450
RAD	0.16%	0.10%	463
RAR-D	0.24%	0.21%	503
*Adam	<b>0.07%</b>	<b>0.05%</b>	461

Table 1: Overview of the mean and standard deviation of the test error and the mean runtime for each sampling method for the Burgers’ equation example.

The mean and standard deviation of the test error and the mean runtime for each sampling method are given in Table 1. Out of the non-adaptive sampling methods tested, only the static uniform grid is unable to capture the solution, resulting in a high test error of 25.9%. The other non-adaptive methods, the static Hammersley grid, and random resampling, attain a significantly lower test error. Overall, our method, in combination with the Adam optimizer, achieves the lowest test error. It achieves a lower error than the next-best sampling method, RAR, at a slightly higher computational cost.

Table 2 compares the performance of the various optimization algorithms for our method in terms of accuracy and efficiency. We note that the performance of nonlinear gradient ascent and the RMSprop optimizers with our proposed method both achieve a competitive test error and computational cost compared to RAR.

Next, we test the behavior of the different sampling methods by varying the number of collocation points from 500 to 20,000; see Figure 2a. We observe that RAR initially reduces the test error the fastest but plateaus at a higher error than the other methods under consideration. PAC-MANN in combination with the Adam optimizer significantly improves the prediction accuracy as the number of collocation points is increased from 1500 to 2000, after which it slowly increases the prediction accuracy. Only at a large number of collocation points (10,000) are the adaptive sampling methods slightly outperformed by the static Hammersley grid.

Sampling method	$L_2$ relative error		Mean runtime [s]	Hyperparameters	
	Mean	1 SD		Stepsize $s$	No. of steps $T$
*Gradient ascent	0.30%	0.17%	<b>436</b>	$10^{-6}$	1
*Nonlinear gradient ascent	0.10%	0.06%	453	$10^{-4}$	5
*RMSprop	0.10%	<b>0.03%</b>	442	$10^{-6}$	10
*Momentum	0.18%	0.24%	448	$10^{-6}$	5
*Adam	<b>0.07%</b>	0.05%	461	$10^{-5}$	15
*Golden section search	0.34%	0.17%	460	$10^{-7}$	5

Table 2: Overview of the mean and standard deviation of the test error and the mean runtime achieved by PACMANN for each optimization algorithm listed in Section 2, including the optimal values for the stepsize and the number of steps, for the Burgers' equation example.

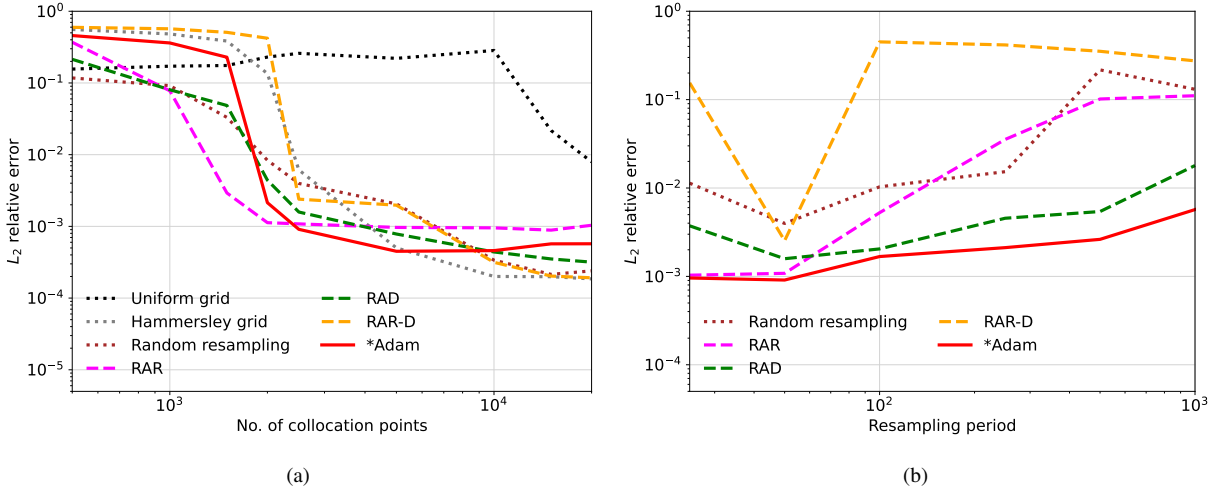


Figure 2: Mean of the test error for each of the sampling methods for a varying (a) number of collocation points and (b) resampling period for the Burgers' equation example.

Figure 2b depicts the behavior of the various sampling methods as the resampling period is increased from 25 to 1000. Generally, most sampling methods lose accuracy as the period is increased. Notably, RAR-D performs significantly better at a period of 50 iterations compared to other resampling periods. PACMANN performs best for all resampling periods considered, losing accuracy slower than the other sampling methods.

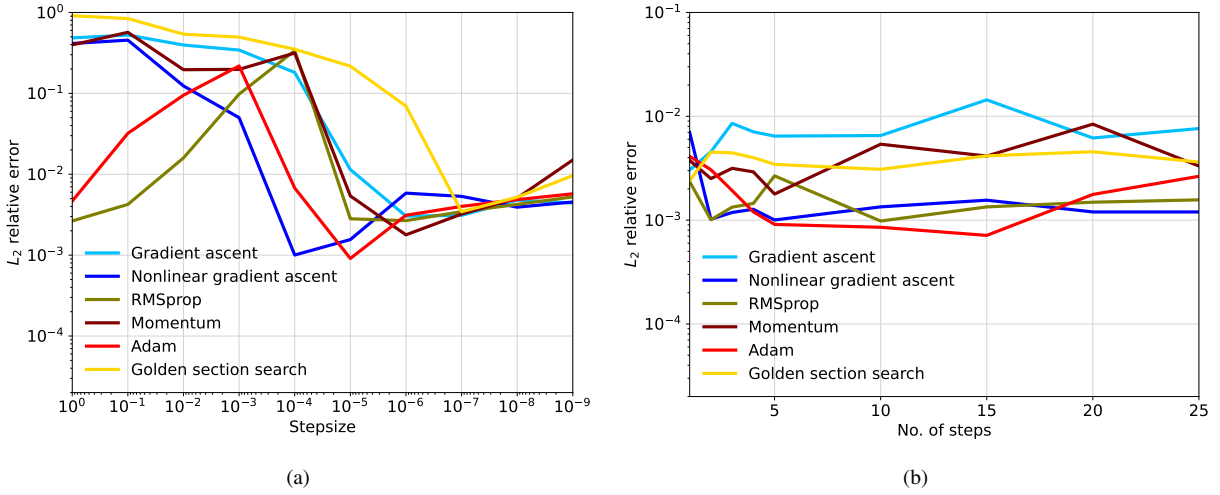


Figure 3: Mean of the test error for PACMANN with the different optimization algorithms listed in Section 2 for a varying (a) stepsize and (b) number of steps for the Burgers' equation example.

In the following, we compare the behavior of the optimizers listed in Section 2 when varying the hyperparameters stepsize  $s$  and number of steps  $T$ . First, in Figure 3a, we test the accuracy of the optimizers for different stepsizes  $s$  ranging from 1 to  $10^{-9}$ . This figure demonstrates that the stepsize has a significant influence on the prediction accuracy achieved by PACMANN. We note that, depending on the optimizer used, a different stepsize is optimal, such as  $10^{-6}$  for momentum or  $10^{-5}$  for Adam. Furthermore, the behavior of the optimizers at stepsizes near 1 is split into two groups, with Adam and RMSprop gaining accuracy as the stepsize is increased, while others continue to lose accuracy. This phenomenon is explained by the number of collocation points that leave the domain while points are moved by PACMANN. At these stepsizes all 2500 collocation points exit the domain when using Adam or RMSprop. Since PACMANN uses a uniform probability distribution to determine the location of the replacement collocation points, the test error approaches the accuracy of random resampling ( $0.40\% \pm 0.35\%$ ). In contrast, when applying the other optimization algorithms with these stepsizes, only a small portion of the collocation points exit the domain, about ten on average. These few points are not significant enough for the random resampling of points to affect the test error achieved. The difference in the number of points that exit the domain may be explained by the relatively large optimal stepsize and number of steps for RMSprop and Adam compared to the other optimization algorithms.

We test the influence of the number of steps  $T$  by ranging it from 1 to 25. Figure 3b shows that certain optimizers benefit from more steps, such as nonlinear gradient ascent and Adam. Others remain at a near-constant accuracy or lose accuracy with additional steps. Based on Figure 3b, we note that the number of steps generally has a smaller impact on the test error achieved compared

to the stepsize.

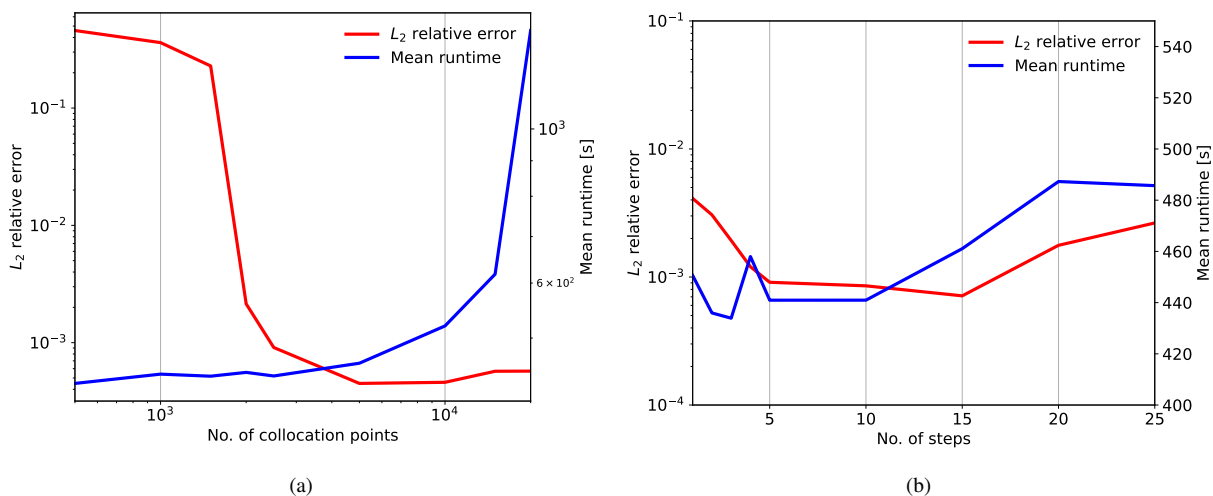


Figure 4: Mean of the test error and the training time for PACMANN with Adam for a varying (a) number of collocation points and (b) number of steps for the Burgers’ equation example.

Furthermore, Figures 4a and 4b depict the prediction accuracy and computational cost of PACMANN with Adam for varying numbers of collocation points and steps. Importantly, we point out that the accuracy of Adam with five steps is nearly the same as its accuracy at 15 steps, however, repeating our method five times is less expensive. Thus, we recommend considering taking fewer steps to save on computational cost in more complex problems.

Next, we compare the distribution of collocation points after training. Figure 5a shows the locations before training when the collocation points are laid out based on the Hammersley sequence. Figures 5b to 5d show the locations of the collocation points after training for RAR, RAD, and PACMANN with Adam, respectively. While RAR creates one large cluster of points at the steepest region of the solution, RAD and our method tend to create several smaller clusters. In contrast to RAD, our method also forms clusters of points in regions with typically lower residuals, indicative of local maxima of the squared residual. We note the similarity between the shape of the clusters and the solution.

### 3.2. 1D Allen-Cahn equation

In the following example, we consider the 1D Allen-Cahn equation:

$$\begin{cases} \frac{\partial u}{\partial t} = d \frac{\partial^2 u}{\partial x^2} + 5(u - u^3), & x \in [-1, 1], \quad t \in [0, 1] \\ u(x, 0) = x^2 \cos(\pi x) \\ u(-1, t) = u(1, t) = -1. \end{cases} \quad (5)$$

Let the diffusion coefficient  $d = 0.001$ . Similar to the previous Burgers’ equation problem, the number of collocation points is set to 2500, the number of boundary points to 80, and the initial

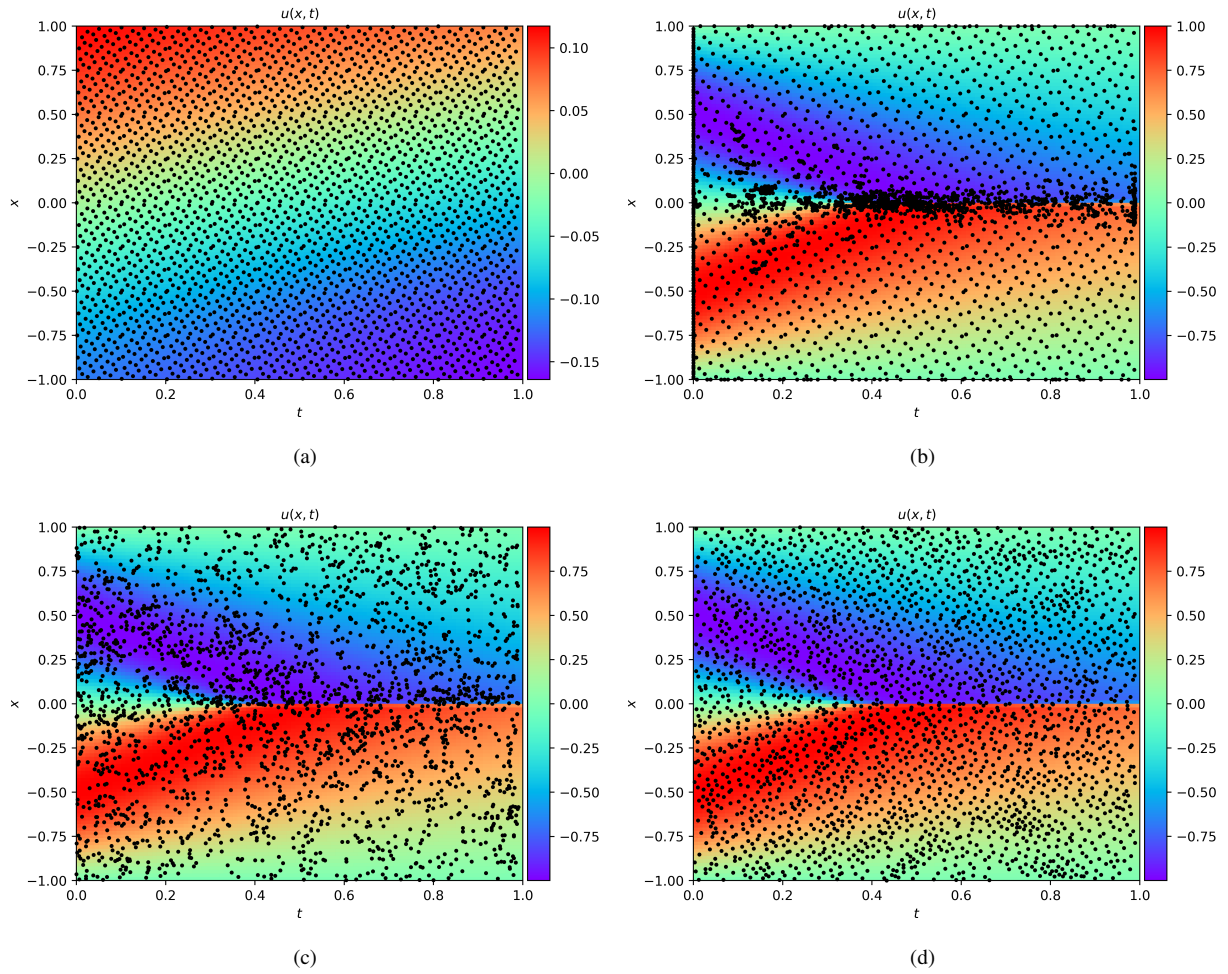


Figure 5: Location of the 2500 collocation points (a) before training and after training with (b) RAR, (c) RAD, and (d) PACMANN with Adam for the Burgers' equation example.

Sampling method	$L_2$ relative error		Mean runtime [s]
	Mean	1 SD	
Uniform grid	44.34%	18.58%	634
Hammersley grid	0.47%	0.26%	<b>591</b>
Random resampling	0.42%	0.28%	592
RAR	0.44%	0.27%	576
RAD	0.93%	0.69%	655
RAR-D	0.28%	0.13%	632
*Adam	<b>0.16%</b>	<b>0.07%</b>	632

Table 3: Overview of the mean and standard deviation of the test error and the mean runtime for each sampling method for the Allen-Cahn equation example.

condition points to 160. The network architecture used for this example consists of four hidden layers of 64 neurons.

The mean and standard deviation of the test error and the mean runtime for each sampling method are given in Table 3. Similarly to the previous Burgers' equation example, the static uniform grid fails to learn the solution and the static Hammersley grid and random resampling offer a significant improvement in accuracy. Out of all sampling methods considered, PACMANN with the Adam optimizer achieves the lowest test error. The next-best method, RAR-D, attains a lower prediction accuracy at the same computational cost. Table 4 demonstrates that Adam results in the lowest mean and standard deviation of the test error for our method in comparison to the other optimization algorithms considered.

Sampling method	$L_2$ relative error		Mean runtime [s]	Hyperparameters	
	Mean	1 SD		Stepsize $s$	No. of steps $T$
*Gradient ascent	0.46%	0.24%	574	$10^{-8}$	5
*Nonlinear gradient ascent	0.42%	0.24%	602	$10^{-7}$	5
*RMSprop	0.29%	0.20%	595	$10^{-6}$	5
*Momentum	0.36%	0.17%	<b>567</b>	$10^{-7}$	5
*Adam	<b>0.16%</b>	<b>0.07%</b>	632	$10^{-5}$	5
*Golden section search	0.37%	0.29%	635	$10^{-7}$	15

Table 4: Overview of the mean and standard deviation of the test error and the mean runtime achieved by PACMANN for each optimization algorithm listed in Section 2, including the optimal values for the stepsize and the number of steps, for the Allen-Cahn equation example.

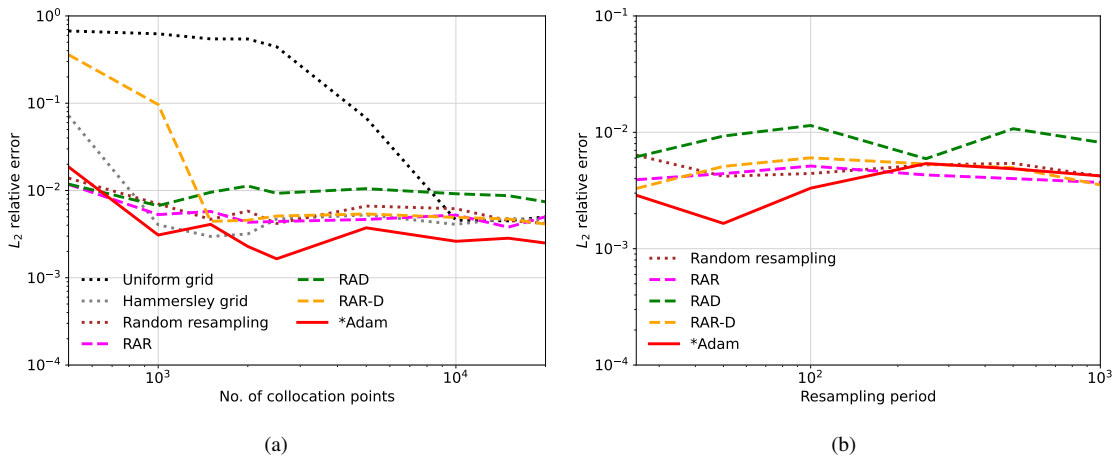


Figure 6: Mean of the test error for each of the sampling methods for a varying (a) number of collocation points and (b) resampling period for the Allen-Cahn equation example.

Figure 6a shows the behavior of the different sampling methods when varying the number of collocation points. We find that PACMANN with the Adam optimizer converges the fastest and

outperforms the other sampling methods for nearly all numbers of collocation points considered. Most sampling methods stagnate above 2500 collocation points, except for the static uniform grid, which requires up to 10,000 collocation points to compete with the accuracy of the other sampling methods.

Moreover, Figure 6b depicts the accuracy of the sampling methods considered for a range of resampling periods. In contrast to our findings in the previous Burgers' equation example, the resampling period has a reduced influence on the test error in this example. Notably, most sampling methods plateau with an increasing resampling period.

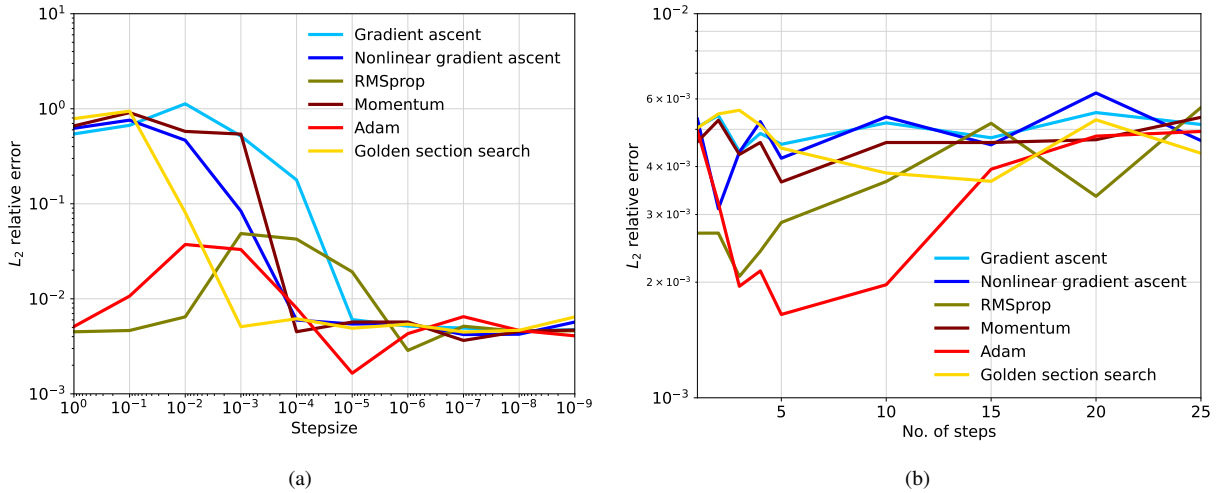


Figure 7: Mean of the test error for PACMANN with the different optimization algorithms listed in Section 2 for a varying (a) stepsize and (b) number of steps for the Allen-Cahn equation example.

Furthermore, we test the behavior of PACMANN with the different optimization algorithms listed in Section 2 by changing the stepsize and the number of steps hyperparameters. Similarly to the previous Burgers' equation example, the stepsize hyperparameter has a significant influence on the test error, as demonstrated by Figure 7a. We note the formation of two groups, which occurs due to the random resampling of points that have been moved outside the domain. When using RMSprop and Adam combined with large stepsizes, all 2500 collocation points leave the domain. As a result, the test error converges toward the error of  $0.42\% \pm 0.28\%$  found when using random resampling.

Finally, we also vary the number of steps. Figure 7b illustrates that the test error of most optimization algorithms is not significantly impacted by changing the number of steps. Figures 7a and 7b support our earlier finding that the stepsize plays a dominant role in the test error obtained compared to the limited influence of the number of steps.

In the following examples, only the Adam optimizer is evaluated for PACMANN since it consistently outperforms the other optimization algorithms. Furthermore, based on the observations made in the previous Burgers' equation example and the current Allen-Cahn equation example, we recommend fixing the number of steps to five, which removes a hyperparameter from PACMANN. We recommend five steps as it takes advantage of the increased accuracy achieved by



our method with the Adam optimizer at multiple steps (see Figures 3b and 7b), while keeping the computational cost low (see Figure 4b).

### 3.3. 5D Poisson’s equation

To demonstrate the feasibility of using PACMANN for higher dimensional problems, we consider the Poisson’s equation in five dimensions:

$$\begin{cases} -\Delta v(\mathbf{x}) = f(\mathbf{x}), & \mathbf{x} \in [-1, 1]^5 \\ v(\mathbf{x}) = 0, & \mathbf{x} \in \partial\Omega. \end{cases} \quad (6)$$

The exact solution is set as

$$v(\mathbf{x}) = \prod_{i=1}^5 \sin(\pi x_i), \quad (7)$$

where  $x_i$  is the  $i$ -th component of  $\mathbf{x}$ . For this example, we sample 750 collocation points and 750 points on the boundary condition. Moreover, the network architecture consists of four hidden layers of 64 neurons each.

Sampling method	$L_2$ relative error		Mean runtime [s]
	Mean	1 SD	
Uniform grid	17.89%	0.94%	742
Hammersley grid	82.08%	3.23%	<b>734</b>
Random resampling	11.03%	0.69%	772
RAR	56.84%	4.46%	753
RAD	10.07%	0.75%	851
RAR-D	88.30%	1.53%	774
*Adam	<b>5.93%</b>	<b>0.46%</b>	778

Table 5: Overview of the mean and standard deviation of the test error and the mean runtime for each sampling method for the Poisson’s equation example.

The mean and standard deviation of the test error and the mean runtime for each of the sampling methods are given in Table 5. In contrast to the previous examples, not only does the static uniform grid fail to capture the solution, but adaptive methods, such as RAR-D, also fail to improve the prediction accuracy. PACMANN in combination with the Adam optimizer and a stepsize of  $10^{-2}$  achieves the lowest mean and standard deviation of the test error. Moreover, we point out the ability of this method to efficiently scale to high-dimensional problems. We find that our method with the Adam optimizer is cheaper at a mean runtime of 778 seconds compared to RAD, the next-best adaptive sampling method, at 851 seconds.

Qualitatively, we observe similar behavior of the different sampling methods when varying the number of collocation points and the resampling period for both the Poisson’s equation example and the following Navier-Stokes equation example, as observed in the Burgers’ equation example.

This observation also applies to the behavior of PACMANN when changing the stepsize and the number of steps hyperparameters. Therefore, for the sake of the length of this paper, we do not repeat the analysis of the behavior of the sampling methods considered in this study for the Poisson’s equation and Navier-Stokes equation examples.

### 3.4. 2D Navier-Stokes equation

Finally, we consider an inverse 2D Navier-Stokes equation problem of an incompressible flow past a cylinder discussed by Raissi et al. in [5], given by:

$$\begin{cases} u_t + \lambda_1(uu_x + vu_y) = -p_x + \lambda_2(u_{xx} + u_{yy}) \\ v_t + \lambda_1(uv_x + vv_y) = -p_y + \lambda_2(v_{xx} + v_{yy}), \end{cases} \quad (8)$$

with  $(x, y) \in [1, 8] \times [-2, 2]$  and  $t \in [0, 7]$ . Here,  $u$  is the x-component of the velocity field, and  $v$  is the y-component. The pressure is denoted by  $p$ . The scalar parameter  $\lambda_1$  scales the convective term, and  $\lambda_2$  represents the dynamic (shear) viscosity. In this example, we are interested in learning the values of the  $\lambda_1$  and  $\lambda_2$  based on a data set created by Raissi et al. [5] containing the values of  $u$ ,  $v$ , and  $p$  determined for a large set of points  $(t, x, y)$ . The true values of  $\lambda_1$  and  $\lambda_2$  are 1 and 0.01, respectively. For this inverse problem, we train the PINN on 7000 randomly selected points from this data set. In addition, we sample 700 collocation points, 200 points on the boundary condition and 100 points on the initial condition. The network architecture consists of six hidden layers containing 50 neurons each.

Sampling method	$L_2$ relative error				Mean runtime [s]
	$\lambda_1$		$\lambda_2$		
	Mean	1 SD	Mean	1 SD	
Uniform grid	0.05%	<b>0.01%</b>	0.72%	0.43%	1506
Hammersley grid	0.08%	0.04%	0.89%	0.52%	<b>1492</b>
Random resampling	0.12%	0.05%	0.65%	0.46%	1514
RAR	0.30%	0.06%	1.44%	0.90%	1520
RAD	0.23%	0.06%	1.38%	0.79%	1583
RAR-D	0.08%	0.05%	0.84%	0.57%	1525
*Adam	<b>0.03%</b>	0.03%	<b>0.53%</b>	<b>0.19%</b>	1559

Table 6: Overview of the mean and standard deviation of the test error for  $\lambda_1$  and  $\lambda_2$  and the mean runtime for each sampling method for the inverse Navier-Stokes equation example.

The mean and standard deviation of the test error for both  $\lambda_1$  and  $\lambda_2$  and the mean training time for each of the sampling methods are given in Table 6. In this inverse problem, PACMANN in combination with Adam at a stepsize of  $10^{-2}$  achieves the lowest test error for  $\lambda_1$  and  $\lambda_2$  at a slightly higher computational cost compared to the following best method, RAR-D. Furthermore, we note that the non-adaptive sampling methods generally outperform the other adaptive methods considered in this study, both in the mean and standard deviation of the test error.

## 4. Conclusions

In this work, we presented PACMANN, a novel adaptive collocation point sampling method for physics-informed neural networks. This approach uses the gradient of the squared residual as guiding information to move collocation points toward areas of large residuals, where the size of the step is determined by the stepsize hyperparameter. Our method can be applied in combination with an optimization algorithm of choice, such as gradient ascent or Adam. Points are moved several times while training is halted, given by the "number of steps" hyperparameter. We explored the sensitivity of our method to its two hyperparameters and we found that the stepsize has a greater influence than the number of steps on the solution accuracy. Conversely, we found that setting the number of steps to 5 achieves the optimal balance between accuracy and efficiency. We then investigated the accuracy and efficiency of PACMANN in combination with various optimization algorithms and concluded that the Adam optimizer performs the best. Furthermore, we compared the performance of PACMANN to existing state-of-the-art adaptive and nonadaptive collocation approaches, including random resampling, RAR and RAD, and demonstrated that our method achieves state-of-the-art performance in terms of accuracy/efficiency tradeoff for lower dimensional benchmarks (1D time-dependent Burgers' and Allen-Cahn equations), while outperforming the state-of-the-art for the five-dimensional Poisson equation. Finally, we showed the effectiveness of our approach to solve inverse problems in a 2D Navier-Stokes benchmark. The results of the numerical experiments demonstrate that PACMANN achieves high prediction accuracy and efficiently scales to higher dimensions without introducing significant computational overhead.

## Appendix A. Relative error behavior of all optimization algorithms considered

This appendix contains figures which describe the behavior of PACMANN in combination with all optimization methods listed in Section 2. Figure A.8a illustrates the prediction accuracy of various optimization algorithms across a range of 500 to 20,000 collocation points in the Burgers' equation example. Overall, the majority of algorithms demonstrate equivalent performance in terms of accuracy. Notably, the golden section search algorithm achieves the lowest error at large numbers of collocation points (20,000 points). Furthermore, we evaluate the behavior of the optimization algorithms for a varying resampling period, from 25 to 1000 iterations, as depicted in Figure A.8b. Most optimization algorithms exhibit a behavior similar to Adam, as highlighted in Section 3. Notably, PACMANN loses prediction accuracy slower for increasing resampling period compared to the other sampling methods.

Similarly, we vary the same hyperparameters for the Allen-Cahn equation example. As shown in Figure A.9a, the other optimization algorithms display behavior comparable to Adam, with prediction accuracy remaining largely unaffected by an increasing number of collocation points. A similar trend is observed for the resampling period in Figure A.9b, where the accuracy shows minimal variation as the number of iterations increases.

## References

- [1] K. Hornik, M. Stinchcombe, H. White, Multilayer feedforward networks are universal approximators, *Neural Networks* 2 (5) (1989) 359–366. doi:10.1016/0893-6080(89)90020-8.

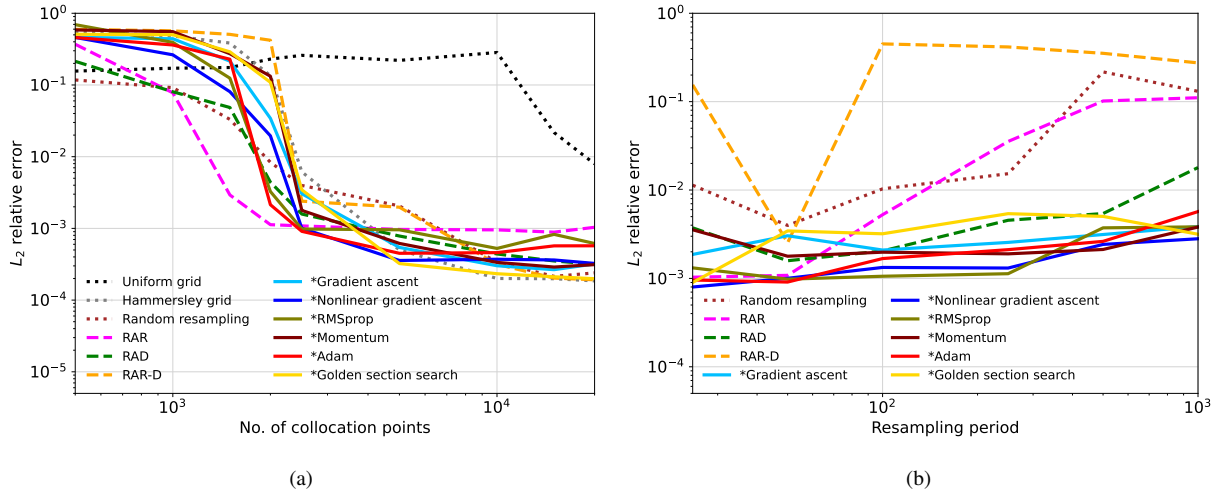


Figure A.8: Mean of the test error for each of the sampling methods and optimization algorithms considered for a varying (a) number of collocation points and (b) resampling period for the Burgers' equation example described in Section 3.

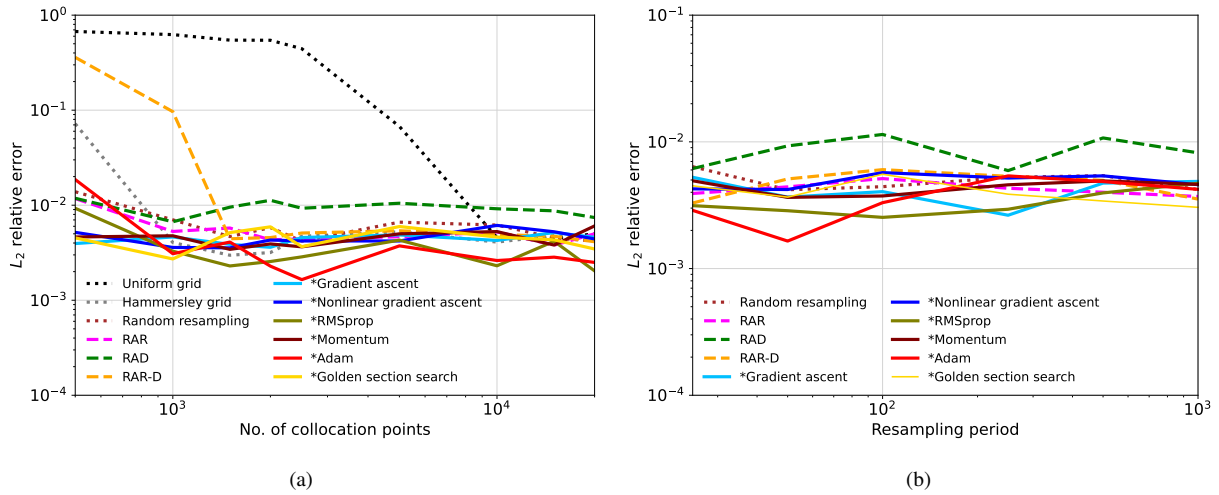


Figure A.9: Mean of the test error for each of the sampling methods and optimization algorithms considered for a varying (a) number of collocation points and (b) resampling period for the Allen-Cahn equation example described in Section 3.

- [2] I. E. Lagaris, A. Likas, D. I. Fotiadis, Artificial neural networks for solving ordinary and partial differential equations, *IEEE transactions on neural networks* 9 (5) (1998) 987–1000. doi:10.1109/72.712178.
- [3] M. W. Dissanayake, N. Phan-Thien, Neural-network-based approximations for solving partial differential equations, *Communications in Numerical Methods in Engineering* 10 (3) (1994) 195–201. doi:10.1002/CNM.1640100303.
- [4] A. Güneş Baydin, B. A. Pearlmutter, A. Andreyevich Radul, J. Mark Siskind, Automatic differentiation in machine learning: a survey, *Journal of Machine Learning Research* 18 (2015) 1–43.
- [5] M. Raissi, P. Perdikaris, G. E. Karniadakis, Physics-informed neural networks: A deep learning framework for solving forward and inverse problems involving nonlinear partial differential equations, *Journal of Computational Physics* 378 (2019) 686–707. doi:10.1016/J.JCP.2018.10.045.
- [6] S. Cuomo, V. S. Di Cola, F. Giampaolo, G. Rozza, M. Raissi, F. Piccialli, Scientific Machine Learning Through Physics-Informed Neural Networks: Where we are and What’s Next, *Journal of Scientific Computing* 2022 92:3 92 (3) (2022) 1–62. doi:10.1007/S10915-022-01939-Z.
- [7] G. E. Karniadakis, I. G. Kevrekidis, L. Lu, P. Perdikaris, S. Wang, L. Yang, Physics-informed machine learning, *Nature Reviews Physics* 2021 3:6 3 (6) (2021) 422–440. doi:10.1038/s42254-021-00314-5.
- [8] Z. Mao, A. D. Jagtap, G. E. Karniadakis, Physics-informed neural networks for high-speed flows, *Computer Methods in Applied Mechanics and Engineering* 360 (2020) 112789. doi:10.1016/J.CMA.2019.112789.
- [9] S. Cai, Z. Wang, F. Fuest, Y.-J. Jeon, C. Gray, G. E. Karniadakis, Flow over an espresso cup: Inferring 3D velocity and pressure fields from tomographic background oriented schlieren videos via physics-informed neural networks, *Journal of Fluid Mechanics* 915 (3 2021). doi:10.1017/jfm.2021.135.
- [10] X. Jin, S. Cai, H. Li, G. E. Karniadakis, NSFnets (Navier-Stokes flow nets): Physics-informed neural networks for the incompressible Navier-Stokes equations, *Journal of Computational Physics* 426 (2021) 109951. doi:10.1016/J.JCP.2020.109951.
- [11] S. Cai, Z. Wang, S. Wang, P. Perdikaris, G. E. Karniadakis, Physics-informed neural networks for heat transfer problems, *Journal of Heat Transfer* 143 (6) (6 2021). doi:10.1115/1.4050542/1104439.
- [12] S. Amini Niaki, E. Haghighat, T. Campbell, A. Poursartip, R. Vaziri, Physics-informed neural network for modelling the thermochemical curing process of composite-tool systems during manufacture, *Computer Methods in Applied Mechanics and Engineering* 384 (2021) 113959. doi:10.1016/J.CMA.2021.113959.
- [13] K. Shukla, P. C. Di Leoni, J. Blackshire, D. Sparkman, G. E. Karniadakis, Physics-informed neural network for ultrasound nondestructive quantification of surface breaking cracks, *Journal of Nondestructive Evaluation* 39 (3) (5 2020). doi:10.1007/s10921-020-00705-1.
- [14] E. Zhang, M. Dao, G. E. Karniadakis, S. Suresh, Analyses of internal structures and defects in materials using physics-informed neural networks, *Science advances* 8 (7) (2 2022). doi:10.1126/SCIADV.ABK0644.
- [15] A. Kovacs, L. Exl, A. Kornell, J. Fischbacher, M. Hovorka, M. Gusenbauer, L. Breth, H. Oezelt, M. Yano, N. Sakuma, A. Kinoshita, T. Shoji, A. Kato, T. Schrefl, Conditional physics informed neural networks, *Communications in Nonlinear Science and Numerical Simulation* 104 (2022) 106041. doi:10.1016/J.CNSNS.2021.106041.
- [16] S. Son, H. Lee, D. Jeong, K. Y. Oh, K. Ho Sun, A novel physics-informed neural network for modeling electromagnetism of a permanent magnet synchronous motor, *Advanced Engineering Informatics* 57 (2023) 102035. doi:10.1016/J.AEI.2023.102035.
- [17] L. Lu, X. Meng, Z. Mao, G. E. Karniadakis, DeepXDE: A Deep Learning Library for Solving Differential Equations, <https://doi.org/10.1137/19M1274067> 63 (1) (2021) 208–228. doi:10.1137/19M1274067.
- [18] M. A. Nabian, R. J. Gladstone, H. Meidani, Efficient training of physics-informed neural networks via importance sampling, *Computer-Aided Civil and Infrastructure Engineering* 36 (8) (2021) 962–977. doi:10.1111/mice.12685.
- [19] C. Wu, M. Zhu, Q. Tan, Y. Kartha, L. Lu, A comprehensive study of non-adaptive and residual-based adaptive sampling for physics-informed neural networks, *Computer Methods in Applied Mechanics and Engineering* 403 (2023) 115671. doi:10.1016/J.CMA.2022.115671.
- [20] J. Guo, H. Wang, C. Hou, A Novel Adaptive Causal Sampling Method for Physics-Informed Neural Networks, *arXiv.org* (2022). doi:10.48550/ARXIV.2210.12914.
- [21] Z. Mao, X. Meng, Physics-informed neural networks with residual/gradient-based adaptive sampling methods

- for solving partial differential equations with sharp solutions, *Applied Mathematics and Mechanics (English Edition)* 44 (7) (2023) 1069–1084. doi:10.1007/S10483-023-2994-7.
- [22] Y. Liu, L. Chen, J. Ding, Y. Chen, An Adaptive Sampling Method Based on Expected Improvement Function and Residual Gradient in PINNs, *IEEE Access* (2024). doi:10.1109/ACCESS.2024.3422224.
- [23] K. Tang, X. Wan, C. Yang, DAS-PINNs: A deep adaptive sampling method for solving high-dimensional partial differential equations, *Journal of Computational Physics* 476 (12 2021). doi:10.1016/j.jcp.2022.111868.
- [24] K. Tang, X. Wan, Q. Liao, Deep density estimation via invertible block-triangular mapping, *Theoretical and Applied Mechanics Letters* 10 (3) (2020) 143–148. doi:10.1016/J.TAML.2020.01.023.
- [25] D. E. Rumelhart, G. E. Hinton, R. J. Williams, Learning representations by back-propagating errors, *Nature* 1986 323:6088 323 (6088) (1986) 533–536. doi:10.1038/323533a0.
- [26] D. P. Kingma, J. L. Ba, Adam: A Method for Stochastic Optimization, 3rd International Conference on Learning Representations, ICLR 2015 - Conference Track Proceedings (12 2014).
- [27] J. M. Hammersley, D. C. Handscomb, *Monte Carlo Methods*, Springer Dordrecht, 1964. doi:10.1007/978-94-009-5819-7.
- [28] G. Hinton, T. Tieleman, Lecture 6.5 - RMSprop: Divide the Gradient by a Running Average of Its Recent Magnitude (2012).
- [29] I. Sutskever, J. Martens, G. Dahl, G. Hinton, On the importance of initialization and momentum in deep learning (5 2013).
- [30] M. J. Kochenderfer, T. A. Wheeler, *Algorithms for optimization*, 1st Edition, The MIT Press, Cambridge, Massachusetts, 2019.
- [31] A. Paszke, S. Gross, F. Massa, A. Lerer, J. Bradbury, G. Chanan, T. Killeen, Z. Lin, N. Gimelshein, L. Antiga, A. Desmaison, A. Köpf, E. Yang, Z. DeVito, M. Raison, A. Tejani, S. Chilamkurthy, B. Steiner, L. Fang, J. Bai, S. Chintala, *PyTorch: An Imperative Style, High-Performance Deep Learning Library*, *Neural Information Processing Systems* (2019).
- [32] Delft High Performance Computing Centre (DHPC), [DelftBlue Supercomputer \(Phase 2\)](https://www.tudelft.nl/dhpc/ark:/44463/DelftBluePhase2) (2024). URL <https://www.tudelft.nl/dhpc/ark:/44463/DelftBluePhase2>